Frequency and Relative Prevalence of Calcium Blips and Puffs in a Model of Small IP_3R Clusters

Hong Qi,[†] Yandong Huang,[†] Sten Rüdiger,[‡] and Jianwei Shuai[†*]
[†]Department of Physics and Institute of Theoretical Physics and Astrophysics, Xiamen University, Xiamen, China; and [‡]Institute of Physics, Humboldt-Universität zu Berlin, Germany

ABSTRACT In this work, we model the local calcium release from clusters with a few inositol 1,4,5-trisphosphate receptor (IP_3R) channels, focusing on the stochastic process in which an open channel either triggers other channels to open (as a puff) or fails to cause any channel to open (as a blip). We show that there are linear relations for the interevent interval (including blips and puffs) and the first event latency against the inverse cluster size. However, nonlinearity is found for the interpuff interval and the first puff latency against the inverse cluster size. Furthermore, the simulations indicate that the blip fraction among all release events and the blip frequency are increasing with larger basal [Ca^{2+}], with blips in turn giving a growing contribution to basal [Ca^{2+}]. This result suggests that blips are not just lapses to trigger puffs, but they may also possess a biological function to contribute to the initiation of calcium waves by a preceding increase of basal [Ca^{2+}] in cells that have small IP_3R clusters.

INTRODUCTION

The calcium ion (Ca^{2+}) acts as a ubiquitous cellular messenger to regulate a wide variety of cellular processes, such as gene expression, neural synapse function, and morphology (1,2). At rest state, cytosolic Ca^{2+} concentration ([Ca^{2+}]) is kept low. When an appropriate stimulus arrives, it can rise rapidly, translating the stimulus into changes in cellular activity. The main mechanism modulating cytosolic [Ca^{2+}] in nonexcitable cells is the Ca^{2+} release through the inositol 1,4,5-trisphosphate receptor (IP_3R) channels localized on the membrane of the endoplasmic reticulum (ER) (3).

The IP_3R channel opens upon binding of inositol 1,4,5-trisphosphate (IP_3), a second messenger generated in response to various extracellular stimuli (4). In addition to its regulation by IP_3, the IP_3R open probability is also modulated by Ca^{2+} in a biphasic manner. A small rise in cytosolic [Ca^{2+}] activates the channel and increases its open probability. This property leads to the process of calcium-induced calcium release (CICR). A further elevation of [Ca^{2+}] will inactivate the channel, resulting in its closure (5,6).

The Ca^{2+} fluorescence experiments indicate that IP_3Rs are nonuniformly distributed on the ER membrane (7–9). In many cell types, the functioning channels are grouped into channel clusters within a domain of hundreds of nanometers (10). The IP_3R clusters are separated by a few micrometers. As a result of this spatial heterogeneity, Ca^{2+} signals display a hierarchical spatiotemporal organization, which ranges from the opening of a single IP_3R (i.e., blips), to concerted activation of a few IP_3Rs within a cluster to generate slightly larger Ca^{2+} elevations (i.e., puffs), and ultimately to global waves via cluster-cluster interactions in response to different IP_3 concentration ([IP_3]) (11,12). Serving as a building block for Ca^{2+} waves at the global level (3) and regulating directly specific physiological functions (12–14), the local Ca^{2+} signals have attracted great experimental and theoretical interest.

For more than a decade, puffs have been extensively studied in *Xenopus* oocyte (7,11) and HeLa cells (8,13). Recently, the quantal properties of local Ca^{2+} releases have been revealed by loading neuroblastoma SH-SY5Y cells (15–18), offering useful insight into specific components of localized calcium events. However, much less is known about the detailed mechanisms of local Ca^{2+} releases modulated by small sizes of channel clusters observed in SH-SY5Y cells, despite that there were many models for puffs in *Xenopus* oocyte (19–24).

In addition to the puff dynamics, the behavior of blips has also been analyzed in experiments with SH-SY5Y cells (15). The experiments in *Xenopus* oocytes discovered few blip events, presumably because of the large number of channels in cluster. However, blips are frequently detected in human neuroblastoma SH-SY5Y cells where a majority of puff sites are composed of 4–6 functional IP_3Rs (15,17). Although there have been simulation studies of blips for single IP_3Rs (24–29), little is known on the blip behavior for a cluster with several IP_3Rs, and especially the possible biological roles of blips. It has remained an open question since the discovery of blips what their biological function could be.

Only recently a few models have been suggested to make a quantitative comparison to the puffs observed in SH-SY5Y cells (17,28–30). In an earlier work, we have used direct numerical simulation of the full three-dimensional (3D) reaction-diffusion system to characterize the distribution of Ca^{2+} in a cluster (24). The major conclusion was that an averaged [Ca^{2+}] based on a mixing assumption of reactants does not hold within an IP_3R cluster (28). A better

Submitted April 23, 2013, and accepted for publication April 15, 2014.

*Correspondence: jianweishuai@xmu.edu.cn

Editor: Godfrey Smith.

0006-3495/14/06/2353/11 $2.00

http://dx.doi.org/10.1016/j.bpj.2014.04.027

but still simple treatment is to separate the high [Ca^{2+}] for an open channel and the averaged (mean field) low [Ca^{2+}] at the closed channels in the cluster. This simple model with two levels of [Ca^{2+}] (28) successfully replicated the distribution of puff amplitudes experimentally observed in SH-SY5Y cell (15).

A stochastic DeYoung-Keizer gating model combined with spatiotemporal dynamics for Ca^{2+} diffusion has been considered for puff dynamics in SH-SY5Y cells (17). However, in the model all channels in the cluster were assigned to a single, central grid element, and so all channels experienced the same local [Ca^{2+}]. In fact, due to the fast diffusion dynamics of intracellular Ca^{2+} ions, the [Ca^{2+}] at the open channel pore is above 100 μM, whereas it decreases below 1 μM at the distance of 1–2 μm from the channel pore (3), having a crucial effect on the stochastic dynamics of channels in a cluster with a radius of several hundred nanometers (26). Ullah et al. (29) simulated spherical Ca^{2+} diffusion dynamics around each open channel and a linearly superposed [Ca^{2+}] to approximate the inhomogeneous distribution of cytosolic calcium in the cluster. The IP_3R gating was modeled by a four-state model constructed with fixed [IP_3] at 10 μM. With the model, they were able to discuss the puff termination dynamics caused by self-inhibition.

In this work, we apply the two-[Ca^{2+}]-level model (28,31) to elucidate dynamics of the stochastic opening of one channel in small clusters either to trigger puffs or to remain as blips. We study systematically the prevalence and frequencies of blips and puffs modified by cluster size, IP_3 concentration, and basal Ca^{2+} concentration. Interestingly, we find nonlinear dependences of interpuff interval (IPI) and first puff latency against the inverse channel number, which were suggested as linear behaviors in an earlier publication (17). A simple theoretical model indicates that a nonlinearity for the IPI appears because more than one channel opens during a puff. However, linear relations occur for the interevent interval (IEI) and the first release event latency against inverse channel number. Furthermore, the model shows that the fraction of blips among all release events is not too small to be neglectable in small clusters, implying that blips may play a biological role for the initiation of waves in cells typically with small clusters.

MODEL

The Ca^{2+} model (28) consists of an ordinary differential equation for the Ca^{2+} concentration and a detailed Markovian model for binding and unbinding processes of Ca^{2+} and IP_3 to IP_3Rs. A modified DeYoung-Keizer model (32) is used here to represent the binding/unbinding dynamics of the IP_3R. In the model, four equivalent and independent subunits are involved in the conduction of an IP_3R. Each subunit has an IP_3 binding site, an activating Ca^{2+} binding site, and an inhibiting Ca^{2+} binding site with transitions governed by on-rates (a_i) and off-rates (b_i) (see Supporting Text S1 for detail in the Supporting Material). A subunit is active when IP_3 and the activating Ca^{2+} sites are occupied but the inactivating site is unoccupied and it is inactive otherwise (32). The channel is defined open if either three or four of the subunits are in the active state.

In (24,28) we have used high-resolution finite-element simulations of the full 3D reaction-diffusion equations for a spatially resolved cluster to understand the subtleties of the cluster geometry. Keeping the cluster radius fixed, we considered varying total channel number N (i.e., cluster size) in the cluster. From the simulations we have concluded that the complexities of intracellular Ca^{2+} distribution can be efficiently reduced by using a coarse-graining approach (28,33). Because of the partial overlap of [Ca^{2+}] profiles around open channels, there are two different [Ca^{2+}] parameters, i.e., $[Ca^{2+}]_{Open}$ and $[Ca^{2+}]_{Close}$, to describe the calcium concentration at open and closed channels, respectively.

When a channel is open, the channel is directly exposed to its own released high [Ca^{2+}], effectively participating in the gating mechanism of this channel. In this study a large concentration $[Ca^{2+}]_{Open} = 120$ μM is used for the open channels. Thus, when a channel switches from the closed state to the open state, the Ca^{2+} concentration will be given immediately by $[Ca^{2+}]_{Open}$.

For a closed channel, the [Ca^{2+}] around its binding sites will be determined by the Ca^{2+} ions diffused from other open channels within the cluster. It has been suggested (28) that the averaged Ca^{2+} concentration at equilibrium ($[Ca^{2+}]_{Equil}$) at the closed channels can be approximated by a linear relationship $[Ca^{2+}]_{Equil} = [Ca^{2+}]_{Rest} + N_{Open}\Delta C$. Here, $[Ca^{2+}]_{Rest}$ is the resting cytosolic [Ca^{2+}], N_{Open} is the number of open channels among all N channels in the cluster, and ΔC is the mean [Ca^{2+}] increment at closed channels resulting from spatial diffusion of Ca^{2+} ions released through an open channel. When a channel switches from the open state to the closed state, the [Ca^{2+}] will be influenced by its diffusion and binding/unbinding with slow buffer EGTA before it reaches the equilibrium value $[Ca^{2+}]_{Equil}$. To incorporate the collapsing dynamics, the following differential equation is considered for the closed channels (31):

$$\frac{d[Ca^{2+}]_{Close}}{dt} = \gamma\left([Ca^{2+}]_{Rest} + N_{Open}\Delta C - [Ca^{2+}]_{Close}\right). \quad (1)$$

Here, γ is the decay rate for domain collapse, which in general depends on many factors such as cluster size and buffer content. Due to the random distribution of closed channels positions, the $[Ca^{2+}]_{Close}$ can be regarded as the average [Ca^{2+}] around the whole cluster, except the sharp peaks of high [Ca^{2+}] around the open channels. Thus, the $[Ca^{2+}]_{Close}$ will be called the domain [Ca^{2+}] in this work.

The on-rates a_i, off-rates b_i, and the dissociation constants d_i of the gating model are related by $d_i = b_i/a_i$, and are determined by fitting the single IP_3R channel patch clamp data (28,34). The detailed channel parameters are given in the Supporting Material, S1. The stochastic bindings and unbindings of IP_3 or Ca^{2+} to the subunits are simulated with two-state Markovian transitions. The time step is fixed at 10 μs, being much shorter than the mean channel open or closed times, whereas data are recorded at each ms.

It has been estimated that a majority of puff sites are composed of 4–6 functional IP_3Rs in neuroblastoma cells, with a wide variability even between sites in a given cell with a few clusters containing 10 or more channels and others with only 2 or 3 (17). In our simulation, we consider channel numbers in a cluster in the range of $N \leq 12$.

We have used experimental results to fit the two important parameters for $[Ca^{2+}]$ dynamics, i.e., ΔC and γ, in Eq.1 (28). A value of $\Delta C = 0.74$ μM was fitted from results of a 3D reaction-diffusion simulation given certain parameters of cluster geometry and calcium binding proteins (28). However, to best fit the experimental data of puff amplitude distribution and puff duration, $\Delta C = 0.3$ μM is required (28). Thus, we select the optimal value ΔC =0.3 μM in our model. The value for $[Ca^{2+}]_{Rest}$ is 0.02 μM if not stated otherwise.

It should be noted that the slow Ca^{2+} binding EGTA used in the experiments modifies the residual calcium after puff release. Furthermore, the stationary and mobile buffers may also affect the channel gating and puff dynamics (35). To account for the effects of Ca^{2+} diffusion, Ca^{2+} pump, and various buffers on Ca^{2+} decay, $\gamma = 1000$ s^{-1} is used for the decay rate of $[Ca^{2+}]$ (31). Thus, the spatial diffusion and the pump and buffer effects have been implicitly implemented into the effective model parameters of ΔC and γ by fitting to the experimental results under the same conditions (28).

RESULTS

Local calcium puffs and blips

Imaged by total internal reflection fluorescence microscopy for SH-SY5Y cells, the Ca^{2+} liberation can be recorded with high resolution at the single channel level. Small rectangular signals (i.e., blips) and larger events (i.e., puffs) of widely varying sizes and amplitudes have been observed. The puffs exhibited abrupt stepwise transitions between fluorescence levels, arising from the recruitment and closing of varying numbers of IP_3Rs.

In the numerical simulation, we can obtain traces of both the domain $[Ca^{2+}]$ and open channel number. Fig. 1 shows the trace of $[Ca^{2+}]_{Close}$ and N_{Open} at $N = 8$ and $[IP_3] = 0.2$ μM, showing both puff and blip events. Puff A in the enlarged drawing consists of an opening of six channels after two channels that open first. This behavior is akin to the triggered puff, i.e., puffs preceded by small, transient $[Ca^{2+}]$ elevations, as observed in experiment (36). Clear stepwise opening and closing of channels are observed during the rising and termination phase for puffs A and B, resulting from the stochastic channel open and closing dynamics.

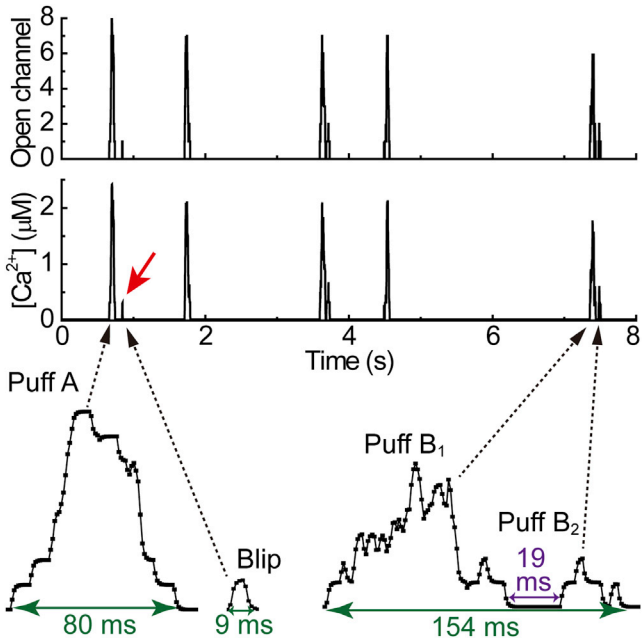

FIGURE 1 The temporal evolution of open channel number (*top*) and the corresponding cluster domain $[Ca^{2+}]$ (*middle*). The red arrow marks a blip. Two puffs (Puff A and Puff B) and a blip are depicted in the enlarged drawing (*bottom*). To see this figure in color, go online.

With the model at given N, $[IP_3]$, and $[Ca^{2+}]_{Rest}$, we run the program for a sufficiently long time to obtain $[Ca^{2+}]_{Close}(t)$ and $N_{Open}(t)$ with a sequence of Ca^{2+} release events. We distinguish blips from puffs by checking the open channel number during a release event. Blips are defined as all events where not more than one channel opens. We then discuss the following mean quantities: the blip fraction, which is defined as the ratio of the blip event number and the number of all release events; the mean blip duration; the blip frequency, which is the inverse of the blip period calculated as the mean interblip interval after ignoring all puff events; and the puff frequency, which is defined as the inverse of the mean IPI after ignoring all blip events.

Effects of cluster size on blips and puffs

In experiments with SH-SY5Y cells, the blip duration is ~17–25 ms (15,37), and the blip fraction among all events observed is ~10–13% with cluster size ~3–8 (37). The puff frequency is in the range of 0.05–2.0 Hz and the mean puff frequency can be fitted with a linear regression to different cluster sizes (17).

For the model the blip fraction is plotted in Fig. 2 *A* as a function of cluster size. The model predicts a large

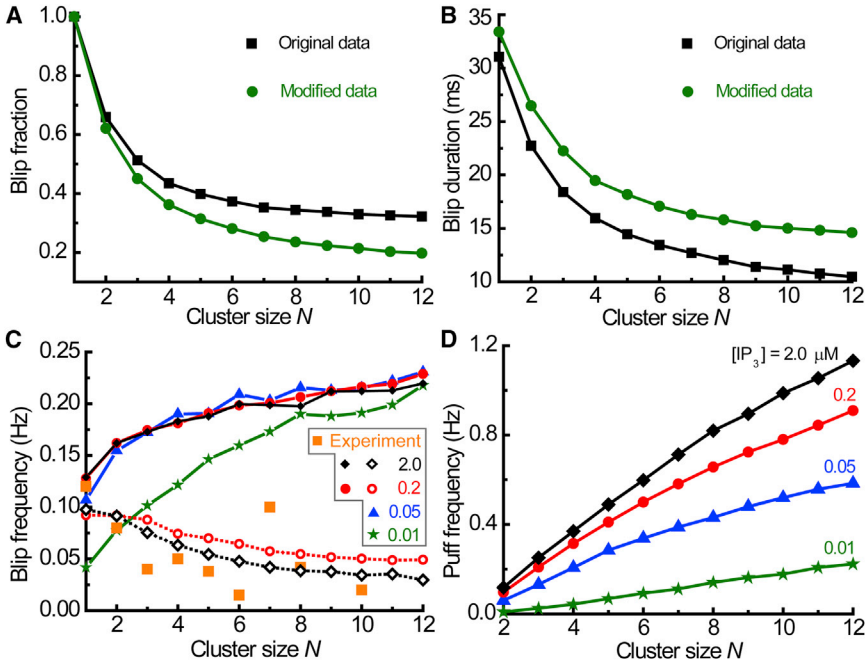

FIGURE 2 (*A*) The blip fraction among all the release events and (*B*) the mean blip duration versus cluster size N with the original data (*squares*) or with the processed data after considering the experimental procedures (*circles*) at $[IP_3] = 0.2\ \mu M$. (*C*) The mean blip frequency against cluster size N. The dashed lines plot the frequency of blip with duration larger than 18 ms. The experimental data in (37) are given by squares. (*D*) The mean puff frequency against cluster size N. Here, $[IP_3] = 0.01$ (*stars*), 0.05 (*triangles*), 0.2 (*circles*), and 2 μM (*lozenges*) in (*C*) and (*D*). To see this figure in color, go online.

probability to find blips, as high as 34% even for a cluster of $N = 8$. The mean duration of blips is plotted in Fig. 2 *B* with squares, giving the mean duration of ~12 ms at $N = 8$, which is shorter than the observed mean blip duration of 17 ms (15). To simulate the situation with strong photo-release of i-IP_3 in experiment, $[IP_3] = 0.2\ \mu M$ is applied here, which is a high concentration for IP_3 binding in the model, because the two IP_3 dissociation constants are $d_1 = 0.005\ \mu M$ and $d_3 = 0.2\ \mu M$.

In our simulation, there are more blips with shorter duration. We exclude the single channel opening events with duration shorter than 6 ms. In the experiment, if two calcium release events are too close to each other, it will be typically counted as a single release event. Thus, in our analysis of simulation data, if all the channels stay closed for <20 ms between two adjacent release events, then the two events are treated as a single release event. As an example shown in Fig. 1, because the two release events B_1 and B_2 are separated by the duration of 19 ms with all channels closed, the B_1 and B_2 events are counted as one puff B.

Furthermore, in experiments long-lasting blips with duration larger than 100 ms can occasionally be observed (15), but were excluded for discussion. The long lifetime blips also occur in our simulation. Following (15), we omit the blips with duration longer than 100 ms, which occur more rarely with larger N. After this procedure, the blip probability is ~23% (Fig. 2 *A*), and the mean blip duration becomes around 16 ms (Fig. 2 *B*) for $N = 8$. In the following we will use these processed data for the discussion of blips and puffs.

The blip frequency and the puff frequency as a function of cluster size N are given in Fig. 2, *C* and *D*, for different $[IP_3]$, respectively. The increasing IP_3R number not only means more channels available to be the first open channel (as a blip or a puff trigger), but also means that more channels are available to be triggered as second channel of the puff. Accordingly, both blip frequency and puff frequency increase with increasing cluster sizes. At small $[IP_3] = 0.01\ \mu M$, the blip frequency is always larger than the puff frequency for any cluster sizes, due to fewer channels binding IP_3 and being available to open. At large $[IP_3] = 2\ \mu M$ with large cluster size, more channels are available to open and the puff frequency increases much more than the blip frequency, giving a small blip fraction.

The model shows that with increasing cluster size the blip frequency increases (Fig. 2 *C*). However, in a recent work by Dickinson and Parker, the experimental data gave a decreasing blip frequency with cluster size (37). Our simulation excludes blips with durations shorter than 6 ms. However, in the experiments of Dickinson and Parker it is likely that blips with durations shorter than 20 ms are significantly undercounted due to background noise (personal communication with George Dickinson at University of California, Irvine, 2014). Considering the experimental resolution, if we exclude the blips with duration shorter than 18 ms, the blip frequency shows a decreasing behavior against cluster size, as plotted in Fig. 2 *C* with open symbols.

The increase of the puff frequency becomes slightly smaller at large cluster sizes, such that the dependence can only roughly be fitted by a linear curve. A linear fitting was observed in experiment with a different statistical method to determine the mean puff frequency (17). In the section Analytical discussion, we will discuss it again in detail by providing a derivation of the functional dependence.

Effects of [IP_3] on blips and puffs

Experimentally, local Ca^{2+} release dynamics modulated by [IP_3] can be studied by changing the ultraviolet flash duration to release different amounts of caged-IP_3. It has been shown that the puff frequency increases progressively with the increasing photo-flash duration (16,17).

With the model we discuss in detail how blips and puffs change with varying [IP_3]. The fraction of blips among all release events against [IP_3] is plotted in Fig. 3 *A* at different cluster sizes. At $N = 1$, all release events are blips. For clusters with $N > 1$, our simulations indicate that the blip fraction decreases with the increase of [IP_3] (Fig. 3 *A*). This is simply because the increasing [IP_3] makes more IP_3Rs available to be opened, resulting in more triggered puffs.

The mean blip duration against [IP_3] is plotted in Fig. 3 *B*. Different relationships of blip duration on [IP_3] are predicted for different N. For the single channel, the mean blip duration increases monotonically with increasing [IP_3], although the mean active time, i.e., the mean time in state (110), is independent of [IP_3] for each IP_3R subunit. At small [IP_3], the open channel typically possesses three active subunits and one nonactive subunit in IP_3-unbound state. With large [IP_3], all four subunits are generally in IP_3-bound states. The channel becomes open with three subunits in the active state and the fourth subunit is typically in the (100) state. The large [Ca^{2+}] will then drive the 4th nonactive subunit into the active state (110). Thus, large [IP_3] causes the channel to open with all four subunits in the active state, resulting in long blip duration.

Differently, for a cluster with several channels, the mean blip duration first increases slightly with increasing [IP_3], and then decreases (Fig. 3 *B*). At $N > 3$, a larger [IP_3] will not only cause the first open channel to stay open longer, but can also induce a puff more easily. The ability for the first open channel to trigger a puff becomes stronger when [IP_3] is larger than the IP_3 dissociation constant $d_1 = 0.005\ \mu$M, generating a decreasing mean blip duration.

The blip frequency versus [IP_3] is displayed in Fig. 3 *C*. At $N = 1$, the blip frequency increases monotonically with increasing [IP_3]. The blip frequency approaches a saturated plateau for [IP_3] $> 0.2\ \mu$M, at which all channel subunits are typically IP_3-bound.

For $N > 3$, the blip frequency shows a biphasic behavior with the increase of [IP_3]. At the small [IP_3] region, before reaching the [IP_3] region where all the subunits are typically IP_3-bound, the increase of [IP_3] will cause not only the increase of puff events, but also the increase of blip events. However, at large [IP_3] many channels are available with IP_3-bound subunits and so the first open channel will easily trigger a puff event, giving rise to a decreasing blip frequency with increasing [IP_3].

Different from the blip frequency shown in Fig. 3 *C*, the puff frequency for a cluster with several channels increases monotonically with increasing [IP_3], approaching to saturation at a very large [IP_3], as plotted in Fig. 3 *D* with $N = 4$. At small [IP_3], due to fewer channels bound with IP_3 for opening, single channel opening events are more frequently observed, giving a larger blip frequency than the puff frequency. Although at large [IP_3], all channels in the cluster are available for opening, and triggered puffs become the dominant release events. As a result, the blip fraction decreases with the increase of [IP_3] (Fig. 3 *A*).

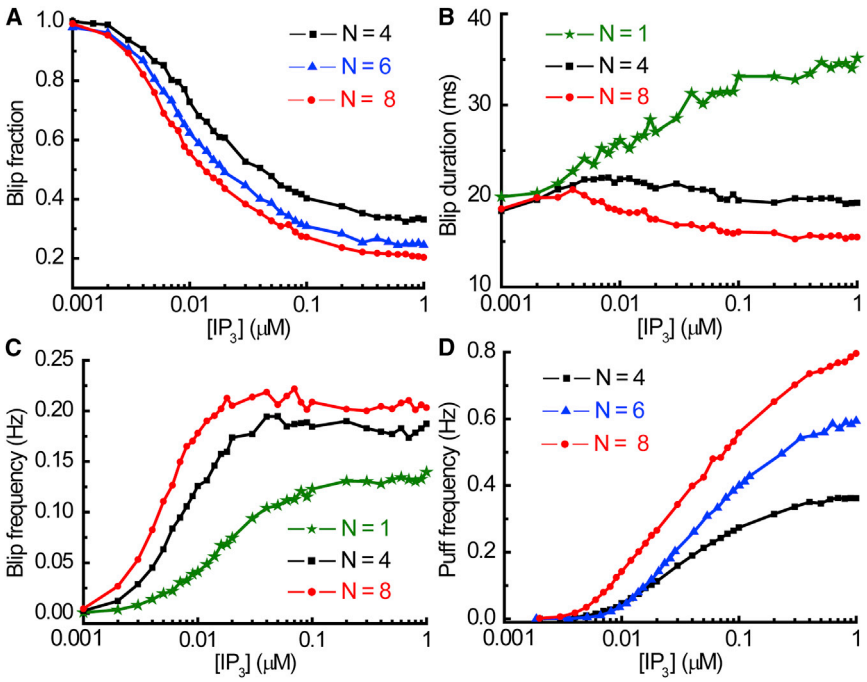

FIGURE 3 (*A*) The blip fraction among all release events, (*B*) the blip duration, (*C*) the blip frequency, and (*D*) the puff frequency as a function of [IP_3] at $N = 1$ (*stars*), 4 (*squares*), 6 (*triangles*), and 8 (*circles*). To see this figure in color, go online.

Effects of basal [Ca^{2+}] on blips and puffs

Before initiating a global Ca^{2+} wave, the Ca^{2+} puffs contribute to a slow rise in basal free [Ca^{2+}] in the cell (38,39). It has been found that the elevated resting [Ca^{2+}] increases the puff frequency and shortens the puff latency (38,39). However, little has been done in experiment to address the effect of basal [Ca^{2+}] on blip dynamics.

In our simulations, we discuss how the blip behavior changes with varying $[Ca^{2+}]_{Rest}$ from 20 to 100 nM at $[IP_3] = 0.2\ \mu M$. The blip fraction against basal [Ca^{2+}] is plotted in Fig. 4 *A*. Fig. 4 *B* shows the blip duration modified by basal [Ca^{2+}]. At first one may expect that similar behaviors should be observed as the effects of [IP_3] on blip frequency and duration given in Fig. 3, *A* and *B*. In particular, one may expect that the blip duration at $N = 1$ will increase with the increase of basal [Ca^{2+}], because the increasing basal [Ca^{2+}] will generate more activation Ca^{2+} binding. Unexpectedly, the simulations suggest that the increase of basal [Ca^{2+}] causes a noticeable linear decrease in blip duration at $N = 1$. A possible explanation for this behavior is that with larger $[Ca^{2+}]_{Rest}$ and the increase in blip frequency, a higher proportion of inhibiting Ca^{2+} binding sites are occupied.

To confirm this hypothesis, we calculate the fraction of Ca^{2+}-inhibited subunits at each event right before the channel becomes open. For $N = 1$ at $[IP_3] = 0.2\ \mu M$, this fraction changes from 0.05 at $[Ca^{2+}]_{Rest} = 0.02\ \mu M$ to 0.14 at $[Ca^{2+}]_{Rest} = 0.1\ \mu M$. A higher fraction of inhibited subunits will then result in a shorter blip duration. The reason for the larger fraction of inhibited subunits may be the short interblip interval, which is below 1 s for $[Ca^{2+}]_{Rest} = 0.1\ \mu M$ (Fig. 4 *C*). In this case, inhibiting Ca^{2+} does not always unbind from the channel before the beginning of the next blip. In fact, the two unbinding times for inhibited Ca^{2+} in the IP_3 model are $1/b_2 = 0.2$ s and $1/b_4 = 8$ s.

For clusters at $N = 4$ and 8, the increase of $[Ca^{2+}]_{Rest}$ leads to a linear and slight decrease in blip duration (Fig. 4 *B*). The blips are those release events where the first open channel fails to trigger more channels to open in the cluster. Thus, the blip duration is limited by the latency between the first open channel and the second open channel. Once a channel first opens as a trigger event, this channel contributes an additional calcium $\Delta C = 0.3\ \mu M$ to the basal [Ca^{2+}] in the cluster domain. With $[Ca^{2+}]_{Rest}$ varying from 0.02 to 0.1 μM, the new basal [Ca^{2+}] for the N-1 closed channels changes from 0.32 to 0.4 μM. The latency to induce the second open channel is relatively insensitive to such a small difference of [Ca^{2+}], resulting in a slightly decreasing blip duration for cluster with several channels.

Fig. 4, *C* and *D*, present the blip frequency and puff frequency against $[Ca^{2+}]_{Rest}$, respectively. With increasing resting [Ca^{2+}], more Ca^{2+} can bind to the activating binding sites of IP_3Rs. Thus, both blips and puffs can occur more frequently. But the increase of the blip event number is larger than that of puff events, resulting in the increase of the blip fraction with increasing basal [Ca^{2+}], as shown in Fig. 4 *A*.

Fig. 4, *C* and *D*, show a positive feedback between local release events and basal [Ca^{2+}], which is in fact a quantitative relation of how CICR works for clustered IP_3Rs. The surprising result in the model that the blip fraction keeps

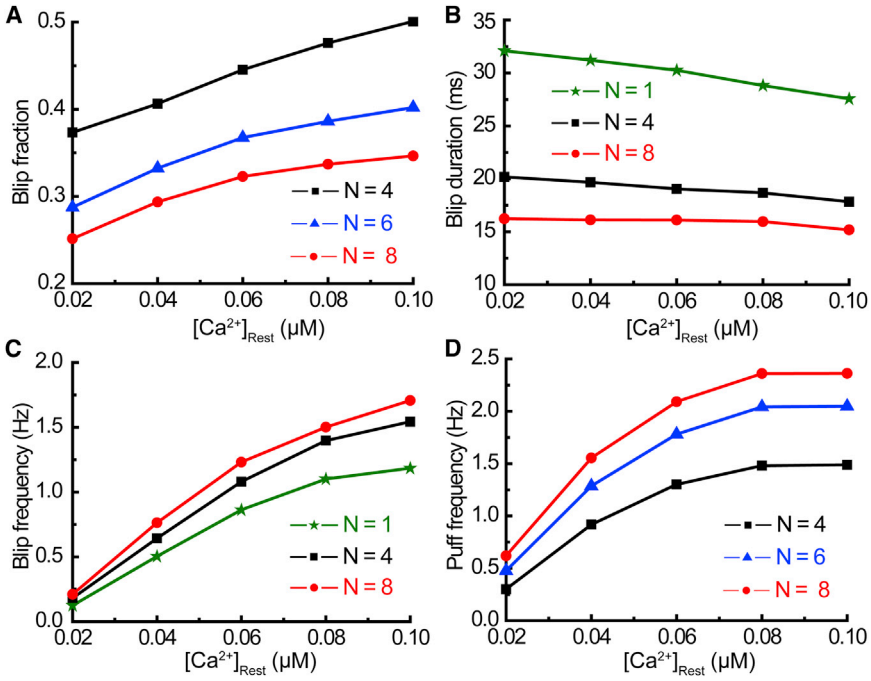

FIGURE 4 (*A*) The blip fraction, (*B*) the blip duration, (*C*) the blip frequency, and (*D*) the puff frequency against basal $[Ca^{2+}]_{Rest}$ for $[IP_3] = 0.2\ \mu M$ at $N = 1$ (*stars*), 4 (*squares*), 6 (*triangles*), and 8 (*circles*). To see this figure in color, go online.

increasing with the increasing basal [Ca^{2+}] indicates an increasing contribution of blips to basal [Ca^{2+}]. This observation gives the blip a possible biological meaning in small cells, which will be discussed in the Discussion.

Mean latency responding to step IP_3

In experiments, the dependence of puff latency on cluster size has been discussed for response to photo-release of i-IP_3 in neuroblastoma cells. It has been shown that the first-puff latency can be fit with a linear regression to reciprocal cluster sizes (17).

In our simulations, we first expose the clustered IP_3Rs in the equilibrium states at zero [IP_3] and resting [Ca^{2+}]. The [IP_3] is then switched to a fixed nonzero value to represent the step increase of photo-release of i-IP_3. The time duration from the onset of IP_3 to the initiation of first puff is then defined as the first-puff latency. In Fig. 5 *A*, the mean first-puff latency is given as a function of 1/*N*. Our simulations reveal a nonlinear relationship between the latency and 1/*N*, which is different from the linear fitting in experiment (17). For comparison, the experimental results of puff latency shown in Fig. 4 of (17) are plotted in Fig. 5 *A* with open red stars.

Note that in the experiment the latency was measured within a limited time (~21 s, personal communication with George Dickinson at University of California, Irvine, 2014). Thus, those latencies that are longer than the experimental observation time will be ignored, which more likely occurs for small clusters $N = 2$ and 3. Accordingly, in our simulation, we discuss the truncated latency with a finite recording time. Here, we consider two finite recording times $T_{rec} = 21$ and 30 s. After disregarding the longer latencies, the truncated mean first-puff latency against 1/*N* is plotted in Fig. 5 *B*. It can be seen that the truncated latencies either can be roughly fitted by linear graphs (for step [IP_3] = 0.05 and 0.2 μM) or still show a nonlinear behavior (for step [IP_3] = 0.01 μM).

With our model we can discuss in detail how the limited recording time T_{rec} affects the puff latency. As shown in the Supporting Material S2, long puff latencies (> 30 s) are occasionally observed for small clusters at $N = 2$, which lengthen the averaged puff latency. The model suggests that a reliable measurement of puff latency requires a recording time longer than 50 s for the cluster with $N = 2$. The simulation results of the latency against cluster size at varying parameters of the calcium decay rate γ and the basal [Ca^{2+}] give similar behaviors as those in Fig. 5, *A* and *B* (see Supporting Material S3).

If, for a single channel, the mean latency of the first release event is T_f, theoretically the latency of the first open channel for a cluster with *N* independent and identical channels is simply given by T_f/N. As plotted in Fig. 5 *A* with open symbols, a linear relationship is obtained with the model between the latency of the first release event (either blips or puffs) and 1/*N*. Thus, the nonlinearity of puff latency is caused by the requirement of at least two channels to be open during a puff (see also Analytical discussion below).

The first puff latency as a function of step [IP_3] is plotted in Fig. 5 *C* at $N = 4$ and 8, as well as the first-blip latency at $N = 1$. At small [IP_3], the latency is mainly determined by the IP_3 binding time, resulting in a decreasing latency with increasing [IP_3]. At large [IP_3], the IP_3 binding time

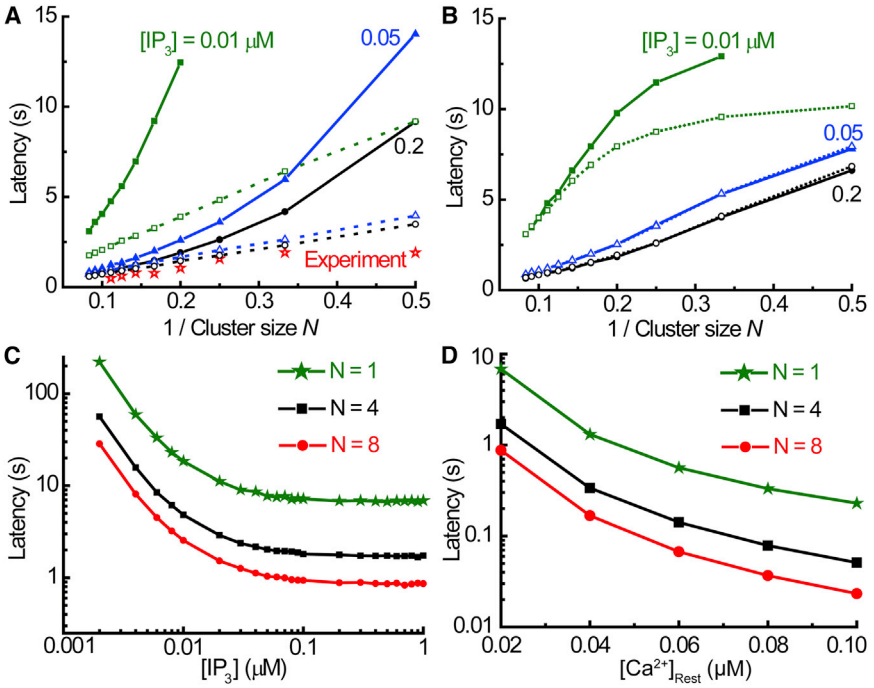

FIGURE 5 The mean latency for clusters in response to step IP_3 increases. (*A*) The first puff-latency (*solid symbols with solid lines*) and the first release event latency (*open symbols with dashed lines*) against reciprocal cluster size 1/*N*. The experimental puff latencies obtained in (17) are plotted with open red stars. (*B*) The latency against 1/*N* for the first puffs responding within 30 s (*solid symbols with solid lines*) and within 21 s (*open symbols with dashed lines*). Here, the step [IP_3] = 0.01 (*squares*), 0.05 (*triangles*), and 0.2 μM (*circles*). The mean first-puff latency at cluster $N = 4$ (*squares*) and 8 (*circles*) and the mean first-blip latency at $N = 1$ (*stars*) as a function of step [IP_3] (*C*) and as a function of resting level $[Ca^{2+}]_{Rest}$ (*D*). To see this figure in color, go online.

is so short that the latency is mainly determined by the Ca^{2+} binding time, showing a saturated latency.

The first puff latency against basal [Ca^{2+}] is shown in Fig. 5 *D* responding to step [IP_3] = 0.2 μM at $N = 4$ and 8, as well as the blip latency at $N = 1$, giving a decreasing behavior with increasing basal [Ca^{2+}].

Analytical discussion of puff events at saturating [IP_3]

In this section, we derive an analytical estimate for the frequency of puff events against the channel number. Furthermore, we compare our simulation and analytical results to the experimental data in (17).

Our analysis assumes that [IP_3] is large enough to saturate the IP_3 binding sites and it starts with an estimate of the rate of single channel opening assuming an initial rest state with zero inhibiting binding site occupancy. For a single receptor channel, the rate for binding of three activating Ca^{2+} is then

$$k_s = 2a_5\left[Ca^{2+}\right]_{Rest}\frac{P_2}{P_0 + P_1 + P_2}, \quad (2)$$

where P_i is the probability that there are i subunits in the active state (110) with $P_0 = (1\text{-}P_{act})^4$, $P_1 = 4\ P_{act}\ (1\text{-}P_{act})^3$, and $P_2 = 6\ P_{act}^2\ (1\text{-}P_{act})^2$ with the probability $P_{act} = a_5\ [Ca^{2+}]_{Rest}/(a_5[Ca^{2+}]_{Rest} + b_5)$ for a single subunit in the active state. $P_2/(P_0 + P_1 + P_2)$ is then the fraction of the receptors being in the state next to the open state, and $2a_5$ $[Ca^{2+}]_{Rest}$ is the flux rate from that state to the open configuration. Eq. 2 expresses the rate out of the closed state (a compound state consisting of the states with 0, 1, or 2 Ca^{2+} bound to the activating site) toward the open state (3 Ca^{2+} bound). With our set of parameters, k_s can be determined to be 0.164 s at $[Ca^{2+}]_{Rest} = 0.02$ μM.

We next consider the fraction of blips, i.e., the fraction of single channel opening that will not result in a puff. Puff failure occurs when during the duration of a blip no further channel opens. The rate of this secondary channel opening will here be denoted by k_2. The probability that a particular second channel does not open during the blip duration τ_m is then given by

$$\rho_2 = \exp(-k_2\tau_m), \quad (3)$$

where τ_m is the average blip duration. From Fig. 3 *B* at largest [IP_3], τ_m is taken here at 0.035 s. The probability for N-1 further channels not to open during the blip duration τ_m is given by

$$\rho = \exp(-(N-1)k_2\tau_m). \quad (4)$$

The average IPI is then given by

$$I = \frac{1}{N \cdot k_s \cdot (1-\rho)} + \tau_{inh}, \quad (5)$$

where τ_{inh} is the average refractory period of a cluster after a puff event. The frequency of events is f = 1/I. The factor 1-ρ reflects the fact that only events with more than a single channel opening should be accounted for. This result indicates that the IPI is not only determined by a factor 1/N, but also modified by 1-ρ, which reflects the requirement for a puff of at least two open channels. For the IEI, which includes both the blips and puffs, we do not consider the factor ρ. Thus, a linear relation occurs for IEI against 1/N.

In Eq. 5, the remaining unknown parameters are k_2 and τ_{inh}. We will determine them from a fitting of IPI against 1/N from our numerical simulations (Fig. 6 *A*). It results that these parameters are given by $k_2 = 14\ s^{-1}$ and $\tau_{inh} = 0.4$ s. Based on our findings, both simulations and theory, the IPI scales in a nonlinear way with inverse cluster size, as shown in Fig. 6 *A*. The simulated data of IEI are also plotted in Fig. 6 *A*, giving a linear relationship, as predicted by the theory.

This nonlinear result for the IPI contridicts the earlier fitting of experimental data shown in Fig. 4 *E* of (17), in which a linear IPI fitting against 1/N is obtained. For comparison, the experimental data are also plotted in Fig. 6 *A* with star symbols. Similar to our discussion of puff latency, we conjecture that in experiments the time of recording of IPIs is too short, especially for the small clusters, and thus the available range of IPIs may be cut off at large values. It has also been pointed out that the underestimations of

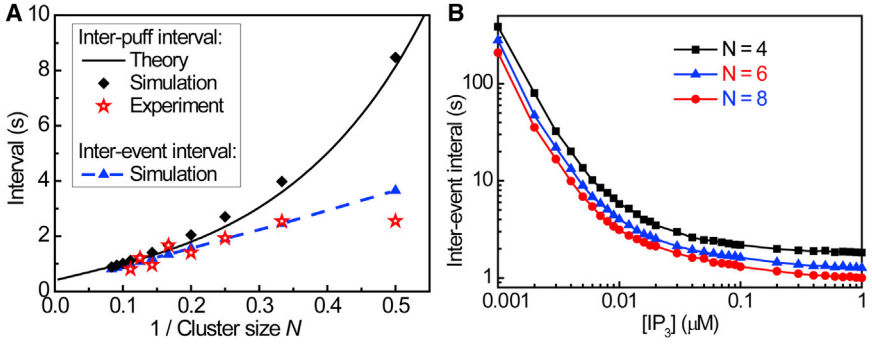

FIGURE 6 (*A*) The IPI against 1/N plotted for simulation results (*squares*), analytical (*line*) results, and experimental data in (17) (*open stars*). The simulation result for the IEI is shown by triangles with a dashed line. In simulation, [IP_3] = 0.2 μM. (*B*) The simulation results of IEI against [IP_3] at $N = 4$ (*squares*), 6 (*triangles*), and 8 (*circles*). To see this figure in color, go online.

the cluster channel number in experiment leads to a systematic underestimation of IPI (17). Note that we think that the overlap between the experimental IPI data and simulation IEI data is accidental.

Here, we use $[IP_3] = 0.2\ \mu M$ in our simulation for the interval calculation. However, the exact value of $[IP_3]$ is unknown in the experiment (17), although a relatively strong flash light has been applied to release the caged IP_3. In Fig. 6 *B* the simulation results of the IEIs against $[IP_3]$ at $N = 4$, 6, and 8 indicate that the IEIs show less sensitivity when $[IP_3] > 0.1\ \mu M$. Thus, simulation results in Fig. 6 *A* at $[IP_3] = 0.2\ \mu M$ are comparable to experimental data with strong flash light.

The simulation results of IPI and IEI against cluster size at varying parameters of $[IP_3]$, the calcium decay rate γ and the basal $[Ca^{2+}]$ exhibit similar behavior (see Supporting Material S4).

DISCUSSION

Recent experiments in neuroblastoma SH-SY5Y cells provided insight into the quantal structure of subcellular Ca^{2+} release events, including both blips and puffs, from clusters with a few IP_3R channels. In this work, we consider a hybrid model to discuss the Ca^{2+} blip dynamics for a cluster of several IP_3R channels. In the model the IP_3R channel gating is represented by stochastic and discrete Markov chains, whereas the spatiotemporal evolution of released Ca^{2+} is tracked in a deterministic way. For the Ca^{2+} evolution, the complexities of intracellular Ca^{2+} reaction and diffusion are condensed into a minimal two-Ca^{2+}-level model (24,28,31). In particular, this reduction takes effectively into account the role of Ca^{2+} binding proteins, such as the EGTA buffer, which was also present in the experiments.

In the work, we study systematically the blip and puff dynamics controlled by various parameters of the cluster model, such as the cluster size, $[IP_3]$ and basal $[Ca^{2+}]$. We here focus on the local calcium releases for small clusters with $N \leq 12$, which so far had been examined less frequently. The blips are those release events where the stochastic opening of one channel fails to trigger other channels to open in the cluster; otherwise, a puff is generated. In fact, whether a blip or a puff occurs depends on IP_3 binding and on the ability of the first open channel to induce the opening of other channels of the cluster through CICR, which depends on the spatial organization of the IP_3Rs inside the cluster. However, we and other authors have argued that collective dynamics of the clustered channels can be captured by the simplified model with mean field description of $[Ca^{2+}]$ around closed channels (24,28,33,40).

Self-inhibition mechanism for channel closure

The two-Ca^{2+}-level model considers a high $[Ca^{2+}]$ at open channels for self-inhibition and an averaged but small $[Ca^{2+}]$ at closed channels for mutual activation. Note that the channel first opens with three subunits in the active state. The large $[Ca^{2+}]$ will then self-activate rapidly the 4th closed subunit, and at a slow timescale the large $[Ca^{2+}]$ will self-inhibit the active subunits of the channel. Thus, our model suggests a self-inhibition dynamics as the mechanism for puff termination, which has been discussed earlier in (15,28,29,31).

Different dynamics to determine the blip duration

The dynamics that determine the blip duration for a single channel or for a cluster of channels are different. For a single channel, in addition to the Ca^{2+} self-inhibition mechanism, the blip duration is also modified by $[IP_3]$ and basal $[Ca^{2+}]$, which determine the availability of active channel subunits. But the blip duration for a cluster of channels is limited by the latency between the first open channel and the second open channel which is triggered by CICR. As a result, the change of blip duration against $[IP_3]$ or basal $[Ca^{2+}]$ shows a more sensitive behavior for a single channel than for a cluster of channels.

Different effects of IP_3 and basal Ca^{2+} on local releases

Although both IP_3 and basal Ca^{2+} can bind to the subunits to open a channel, our simulations indicate that the behaviors for blip fraction and frequency against $[IP_3]$ are different from those against basal $[Ca^{2+}]$. With increasing $[IP_3]$, the blip fraction decreases because more channels become available and so more release events are triggered puffs. Differently, the blip fraction increases with increasing basal $[Ca^{2+}]$ because more subunits of channels become inhibited and so more release events are only blips.

Cluster size modified IPI and the first puff latency

The model shows that with increasing cluster size the puff frequency increases rapidly and the frequency of blips with duration larger than 6 ms increase slightly. However, in a recent work by Dickinson and Parker, the experimental data gave a decreasing blip frequency with cluster size (37). In the experiments of Dickinson and Parker it is likely that blips with durations shorter than 20 ms are significantly undercounted due to background noise (personal communication with George Dickinson at University of California, Irvine, 2014). Besides the simplicity of the model, we think, this discrepancy is also related to the different data processing. Our simulation results excluding blips with durations shorter than 18 ms show a similar behavior as observed in experiment.

Our simulations show that the mean IPI has a nonlinear relationship against the inverse cluster size. The analytic

results indicate that a linear dependence occurs between IEI and 1/N. Modified by a factor that reflects the fact of more than one channel opening during a puff, the IPI gives a nonlinear relationship with $1/N$. The model also shows that the mean first-puff latency has a nonlinear relationship against the reciprocal cluster size. Theoretically, assuming that the channels are identical and independent, there is a linear relationship between the mean latency of the first release event and the inverse cluster size.

The nonlinear behaviors for the IPI and puff latency with the model contradict the earlier fitting of experimental data shown in (17) in which a linear regression has been suggested for $N \geq 3$. A recent model also suggested a linear relationship between IPI and cluster size for $N \geq 3$ (41). Although our simulation IPI data plotted in Fig. 6 *A*, Figs. S5 *A*, S6 *A*, and S7 *A* could also roughly be fitted by linear functions against N at $N \geq 3$, the nonlinear behavior is obvious when including the data for $N = 2$. The nonlinear fit is robust for the variation of model parameters as shown in the Supporting Material.

The experiments deal with complex situations, which cannot completely be accounted for by a simple model and theory. The experimental recording occurs within a limited time that is typically around 21 s. The experimental results are averaged for many cluster sites with different geometric distributions of channels. The basal calcium can increase due to Ca^{2+} release from nearby clusters. In addition to the channel noise, various sources of noise are present in the cell.

Although the experimental accuracy can be limited by insufficient statistics, and the model involves many simplifications, the discrepancy between our simulations and experiments raises an interesting question for a future study. As a fact, our model, as well as the mathematical theory, ignores many factors, including the spatial diffusion, the nonlinear calcium pump, different types of Ca^{2+} buffers, and the interaction with other clusters. Thus, a more realistic Ca^{2+} model should be considered and discussed. For example, it has been shown that the dye buffer will affect puff amplitude largely (41,42), and fast mobile buffer can increase the channel number involved in a puff (35). To what extent the buffer can modulate the IPI and release duration is an interesting question for further study. Such a discrepancy may also suggest that, rather than the independent channels, a direct biochemical coupling mechanism could exist to influence cooperative opening and closing for adjacent channels. Based on our simulations, the $N = 2$ cluster plays a crucial role to check the nonlinearity of puff latency and IPI against $1/N$. We suggest that recording time in experiments for IPI and latency discussion should be performed with the recording time longer than 50 s, which is required for a minimal cluster with $N = 2$.

The possible role of blips to enhance basal [Ca^{2+}] and initiate Ca^{2+} waves

For *Xenopus* oocyte cells, each cluster typically has ~20–35 IP_3Rs (36,43). With such a large cluster, the first open channel will easily lead nearby IP_3Rs to open due to CICR. Thus, triggered puffs are typically observed with less blips in the large *Xenopus* oocytes (36). Blips simply fail to trigger puffs and may play less of a biological role in large cells. However, in small cells, such as neuroblastoma, with only several clusters on the ER typically composed of 4–6 functional IP_3Rs (17), our simulations suggest that the blips may play a role for the initiation of waves. For a cluster with 4–6 IP_3Rs, the model shows that the fraction of blips among all release events can be larger than 30%. Thus, besides puffs, the blip events could contribute a significant portion to the increase of basal [Ca^{2+}].

A surprising result with the model is that, besides the blip frequency, the blip fraction among all release events keeps increasing with increasing basal [Ca^{2+}]. Thus, there is a positive feedback loop between blip releases and basal [Ca^{2+}], giving an increasing contribution of blips to basal [Ca^{2+}]. This observation indicates that the blips are not only a failure to trigger puffs. It has remained an open question since the discovery of blips what their biological function could be. According to our investigation, we suggest that by a contribution to increase basal [Ca^{2+}] the blips may possibly participate in the initiation of calcium waves, especially in cells with small clusters, such as neuroblastoma (17). Thus, it may be biologically very relevant to discuss the blip dynamics in small cells.

SUPPORTING MATERIAL

Seven figures and supporting text are available at http://www.biophysj.org/biophysj/supplemental/S0006-3495(14)00444-5.

We acknowledge many useful conversations with Ian Parker and George Dickinson.

J.S. acknowledge support from the China National Funds for Distinguished Young Scientists under grant 11125419, the National Natural Science Foundation of China under grant 31370830, the Fujian Province Funds for Leading Scientist in Universities, and the ICAM branches cost sharing fund. S.R. acknowledges support by the Deutsche Forschungsgemeinschaft. Computational support from the Key Laboratory for Chemical Biology of Fujian Province, Xiamen University, and Xiamen Super Computing Center are gratefully acknowledged.

REFERENCES

1. Berridge, M. J. 1997. Elementary and global aspects of calcium signalling. *J. Exp. Biol.* 200:315–319.

2. Berridge, M. J., M. D. Bootman, and P. Lipp. 1998. Calcium—a life and death signal. *Nature.* 395:645–648.

3. Foskett, J. K., C. White, …, D. O. D. Mak. 2007. Inositol trisphosphate receptor Ca^{2+} release channels. *Physiol. Rev.* 87:593–658.

4. Mikoshiba, K. 2007. The IP_3 receptor/Ca^{2+} channel and its cellular function. *Biochem. Soc. Sympos.* 74:9–22.
5. Bezprozvanny, I., J. Watras, and B. E. Ehrlich. 1991. Bell-shaped calcium-response curves of Ins(1,4,5)P_3- and calcium-gated channels from endoplasmic reticulum of cerebellum. *Nature.* 351:751–754.
6. Finch, E. A., T. J. Turner, and S. M. Goldin. 1991. Calcium as a coagonist of inositol 1,4,5-trisphosphate-induced calcium release. *Science.* 252:443–446.
7. Yao, Y., J. Choi, and I. Parker. 1995. Quantal puffs of intracellular Ca^{2+} evoked by inositol trisphosphate in *Xenopus* oocytes. *J. Physiol.* 482:533–553.
8. Bootman, M. D., and M. J. Berridge. 1996. Subcellular Ca^{2+} signals underlying waves and graded responses in HeLa cells. *Curr. Biol.* 6:855–865.
9. Sun, X. P., N. Callamaras, …, I. Parker. 1998. A continuum of $InsP_3$-mediated elementary Ca^{2+} signalling events in *Xenopus* oocytes. *J. Physiol.* 509:67–80.
10. Wiltgen, S. M., I. F. Smith, and I. Parker. 2010. Superresolution localization of single functional IP_3R channels utilizing Ca^{2+} flux as a readout. *Biophys. J.* 99:437–446.
11. Parker, I., J. Choi, and Y. Yao. 1996. Elementary events of $InsP_3$-induced Ca^{2+} liberation in *Xenopus* oocytes: hot spots, puffs and blips. *Cell Calcium.* 20:105–121.
12. Berridge, M., P. Lipp, and M. Bootman. 1999. Calcium signalling. *Curr. Biol.* 9:R157–R159.
13. Bootman, M., E. Niggli, …, P. Lipp. 1997. Imaging the hierarchical Ca^{2+} signalling system in HeLa cells. *J. Physiol.* 499:307–314.
14. Bootman, M. D., P. Lipp, and M. J. Berridge. 2001. The organisation and functions of local Ca^{2+} signals. *J. Cell Sci.* 114:2213–2222.
15. Smith, I. F., and I. Parker. 2009. Imaging the quantal substructure of single IP_3R channel activity during Ca^{2+} puffs in intact mammalian cells. *Proc. Natl. Acad. Sci. USA.* 106:6404–6409.
16. Smith, I. F., S. M. Wiltgen, and I. Parker. 2009. Localization of puff sites adjacent to the plasma membrane: functional and spatial characterization of Ca^{2+} signaling in SH-SY5Y cells utilizing membrane-permeant caged IP_3. *Cell Calcium.* 45:65–76.
17. Dickinson, G. D., D. Swaminathan, and I. Parker. 2012. The probability of triggering calcium puffs is linearly related to the number of inositol trisphosphate receptors in a cluster. *Biophys. J.* 102:1826–1836.
18. Dickinson, G. D., and I. Parker. 2013. Temperature dependence of IP_3-mediated local and global Ca^{2+} signals. *Biophys. J.* 104:386–395.
19. Shuai, J. W., and P. Jung. 2002. Optimal intracellular calcium signaling. *Phys. Rev. Lett.* 88:068102.
20. Shuai, J. W., and P. Jung. 2003. Selection of intracellular calcium patterns in a model with clustered Ca^{2+} release channels. *Phys. Rev. E Stat. Nonlin. Soft Matter Phys.* 67:031905.
21. Thul, R., and M. Falcke. 2004. Release currents of IP_3 receptor channel clusters and concentration profiles. *Biophys. J.* 86:2660–2673.
22. Groff, J. R., and G. D. Smith. 2008. Calcium-dependent inactivation and the dynamics of calcium puffs and sparks. *J. Theor. Biol.* 253:483–499.
23. Zeller, S., S. Rüdiger, …, M. Falcke. 2009. Modeling of the modulation by buffers of Ca^{2+} release through clusters of IP_3 receptors. *Biophys. J.* 97:992–1002.
24. Rüdiger, S., Ch. Nagaiah, …, J. W. Shuai. 2010. Calcium domains around single and clustered IP_3 receptors and their modulation by buffers. *Biophys. J.* 99:3–12.
25. Swillens, S., P. Champeil, …, G. Dupont. 1998. Stochastic simulation of a single inositol 1,4,5-trisphosphate-sensitive Ca^{2+} channel reveals repetitive openings during 'blip-like' Ca^{2+} transients. *Cell Calcium.* 23:291–302.
26. Rüdiger, S., J. W. Shuai, …, M. Falcke. 2007. Hybrid stochastic and deterministic simulations of calcium blips. *Biophys. J.* 93:1847–1857.
27. Shuai, J., J. E. Pearson, and I. Parker. 2008. Modeling Ca^{2+} feedback on a single inositol 1,4,5-trisphosphate receptor and its modulation by Ca^{2+} buffers. *Biophys. J.* 95:3738–3752.
28. Rüdiger, S., J. W. Shuai, and I. M. Sokolov. 2010. Law of mass action, detailed balance, and the modeling of calcium puffs. *Phys. Rev. Lett.* 105:048103.
29. Ullah, G., I. Parker, …, J. E. Pearson. 2012. Multi-scale data-driven modeling and observation of calcium puffs. *Cell Calcium.* 52:152–160.
30. Rüdiger, S. 2014. Stochastic models of intracellular calcium signals. *Phys. Rep.* 534:39–87.
31. Rüdiger, S., P. Jung, and J. W. Shuai. 2012. Termination of Ca^{2+} release for clustered IP_3R channels. *PLOS Comput. Biol.* 8:e1002485.
32. De Young, G. W., and J. Keizer. 1992. A single-pool inositol 1,4,5-trisphosphate-receptor-based model for agonist-stimulated oscillations in Ca^{2+} concentration. *Proc. Natl. Acad. Sci. USA.* 89:9895–9899.
33. Nguyen, V., R. Mathias, and G. D. Smith. 2005. A stochastic automata network descriptor for Markov chain models of instantaneously coupled intracellular Ca^{2+} channels. *Bull. Math. Biol.* 67:393–432.
34. Shuai, J. W., D. P. Yang, …, S. Rüdiger. 2009. An investigation of models of the IP_3R channel in *Xenopus* oocyte. *Chaos.* 19:037105.
35. Fraiman, D., and S. P. Dawson. 2014. Buffer regulation of calcium puff sequences. *Phys. Biol.* 11:016007.
36. Rose, H. J., S. Dargan, …, I. Parker. 2006. 'Trigger' events precede calcium puffs in *Xenopus* oocytes. *Biophys. J.* 91:4024–4032.
37. Dickinson, G. D., and I. Parker. 2013. Factors determining the recruitment of inositol trisphosphate receptor channels during calcium puffs. *Biophys. J.* 105:2474–2484.
38. Marchant, J., N. Callamaras, and I. Parker. 1999. Initiation of IP_3-mediated Ca^{2+} waves in Xenopus oocytes. *EMBO J.* 18:5285–5299.
39. Yamasaki-Mann, M., A. Demuro, and I. Parker. 2013. Cytosolic [Ca^{2+}] regulation of $InsP_3$-evoked puffs. *Biochem. J.* 449:167–173.
40. DeRemigio, H., J. R. Groff, and G. D. Smith. 2007. The spatial organization of calcium release sites and the dynamics of puffs and sparks. Biophysical Society Annual Meeting Abstracts. Program No. 1211, Baltimore, MD. 256A.
41. Cao, P., G. Donovan, …, J. Sneyd. 2013. A stochastic model of calcium puffs based on single-channel data. *Biophys. J.* 105:1133–1142.
42. Solovey, G., D. Fraiman, and S. P. Dawson. 2011. Mean field strategies induce unrealistic non-linearities in calcium puffs. *Front. Physiol.* 2:46.
43. Shuai, J. W., H. J. Rose, and I. Parker. 2006. The number and spatial distribution of IP_3R receptors underlying calcium puffs in Xenopus oocytes. *Biophys. J.* 91:4033–4044.